

On the Mechanistic Understanding of Photovoltage Loss in Iron Pyrite Solar Cells

Mohammad Rahman,* Gerrit Boschloo, Anders Hagfeldt, and Tomas Edvinsson*

Considering the natural abundance, the optoelectronic properties, and the electricity production cost, iron pyrite (FeS_2) has a strong appeal as a solar cell material. The maximum conversion efficiency of FeS_2 solar cells demonstrated to date, however, is below 3%, which is significantly below the theoretical efficiency limit of 25%. This poor conversion efficiency is mainly the result of the poor photovoltage, which has never exceeded 0.2 V with a device having appreciable photocurrent. Several studies have explored the origin of the low photovoltage in FeS_2 solar cells, and have improved understanding of the photovoltage loss mechanisms. Fermi level pinning, surface inversion, ionization of bulk donor states, and photocarrier loss have been suggested as the underlying reasons for the photovoltage loss in FeS_2 . Given the past and more recent scientific data, together with contradictory results to some extent, it is timely to discuss these mechanisms to give an updated view of the present status and remaining challenges. Herein, the current understanding of the origin of low photovoltage in FeS_2 solar cells is critically reviewed, preceded by a succinct discussion on the electronic structure and optoelectronic properties. Finally, suggestions of a few research directions are also presented.

solar cell application. For example, it has a bandgap of ≈ 0.95 eV (to attain a solar energy conversion efficiency up close to the Shockley–Queisser limit), high minority carrier diffusion lengths (100–1000 nm), a high absorption coefficient commensurate with thin film thickness for complete light absorption (a 100 nm thick film absorbs $>90\%$ of sunlight under the bandgap), and an electron mobility of up to $360 \text{ cm}^2 \text{ V}^{-1} \text{ s}^{-1}$ at room temperature.^[1–3] Therefore, FeS_2 bears great promises for application in solar cells, particularly, to be used as a thin-film solar cell material alongside currently used thin-film photovoltaic (PV) materials, such as CdTe, $\text{CuIn}_{1-x}\text{Ga}_x\text{Se}_2$ (CIGS), and hybrid perovskites.

FeS_2 offers possibilities of the lowest-priced electricity production among the known solar cell materials.^[4] In a comparative study,^[4] a list of 23 candidate materials including Si was evaluated in terms

1. Introduction

Iron pyrite (FeS_2) has electronic and optical properties that seemingly make it a very promising absorber material for

of annual electricity production potential (TW) and production cost (€ per W). FeS_2 outstands all of them. Most importantly, FeS_2 outweighs Si in every aspects. Some key issues that favor FeS_2 over Si are: the energy input for extraction (24 kWh kg^{-1} for Si vs 2 kWh kg^{-1} for Fe), extraction cost ($\$1.70$ per kg for Si vs $\$0.03$ per kg for Fe), photon flux absorption coefficient (FeS_2 has two orders of magnitude higher absorption coefficient), and a low levelized cost of the raw material per peak Watt (0.039 € per W for Si vs $<0.000002 \text{ € per W}$ for FeS_2).^[4,5] It is therefore argued that a 4% efficient FeS_2 solar cell would produce the output at a comparable price as that of a 19% efficient Si-based solar cell.^[4] Noticeably, the costs of Si production have showed a decreasing trend and new alternative thin film PV materials (hybrid perovskites and copper zinc tin sulfide, CZTS) have emerged. However, the intrinsic materials consumption as well as the extraction cost are still very low for FeS_2 . If FeS_2 is produced in the same country with the same wages, electricity price, and tax policies that are set for Si; the use of FeS_2 in a PV technology has predicted to be more cost-effective than Si. With the cost for producing modules with interconnects/framing and additional system costs for installation that scales with solar cell area, however, the power conversion efficiency (PCE) has to be significantly higher than 4% to be competitive. As the raw material cost is a quite small part of the total module and system cost, it is likely that FeS_2 has to reach efficiencies close to existing thin film materials to be economically competitive.


Since its first demonstration,^[6] despite this high recognition and an intermittent research efforts of over three decades,

Dr. M. Rahman, Prof. T. Edvinsson
Department of Engineering Sciences
Division of Solid State Physics

Angstrom Laboratory
Uppsala University
Uppsala 751 21, Sweden
E-mail: mohammad.rahman@angstrom.uu.se;
tomas.edvinsson@angstrom.uu.se

Prof. G. Boschloo
Department of Chemistry
Angstrom Laboratory
Uppsala University
Uppsala 751 20, Sweden

Prof. A. Hagfeldt
Laboratory for Photomolecular Science
École Polytechnique Fédérale de Lausanne
Lausanne CH-1015, Switzerland

 The ORCID identification number(s) for the author(s) of this article can be found under <https://doi.org/10.1002/adma.201905653>.

© 2020 The Authors. Published by WILEY-VCH Verlag GmbH & Co. KGaA, Weinheim. This is an open access article under the terms of the Creative Commons Attribution-NonCommercial License, which permits use, distribution and reproduction in any medium, provided the original work is properly cited and is not used for commercial purposes.

DOI: 10.1002/adma.201905653

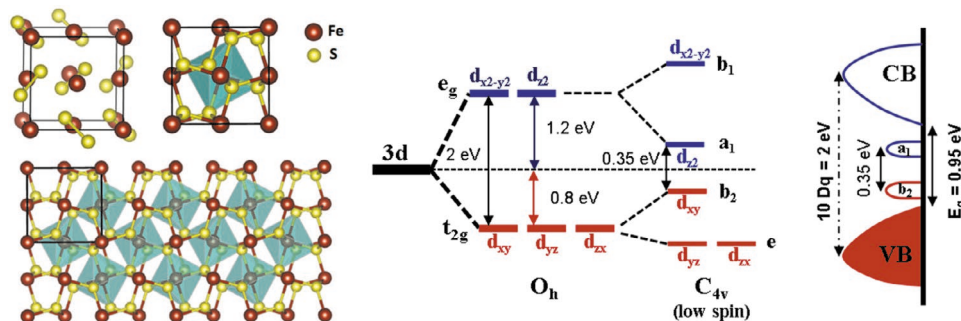


Figure 1. Left) Unit cell structure of cubic pyrite with Pa-3 symmetry showing the sulfur pairs, octahedral coordination of Fe–S, and relative octahedral tilting. Right) Fe 3d ligand field splitting due to symmetry reduction from O_h to square pyramidal C_{4v} at the surface. Ligand field splitting depicted using data from ref. [24].

however, FeS₂ solar cells never have exceeded a PCE greater than 2.8%. This value was attained in a photoelectrochemical cell with a liquid junction I⁻/I₃⁻ electrolyte and any PCE has not yet been certified in an accredited laboratory, while solid-state devices so far show significantly lower PCE. The low PCE is mainly due to the extremely poor open-circuit voltage, V_{OC} (typically <200 mV).^[1,7] Secondary phases, surface conduction phenomena, and undesired doping have been reported as the key issues behind this poor conversion efficiency^[7–13] that subsequently lead to phenomena, such as surface inversion,^[7] ionization of deep donor states,^[10] and photocarrier recombination^[14] for loss of photovoltage.

It is speculated that if the efficiency would improve to 10%, the estimated production cost of electricity with FeS₂ would be as low as <0.000002 ¢ per W, an unbeatable price for any known solar cells materials at this time.^[4] Apparently, a 10% efficiency for FeS₂ looks far beyond the reality, and as we argue above from a total module and system cost, the efficiencies would likely need to approach already implemented thin film materials. If the V_{OC} would be improved to 500 mV, however, a conversion efficiency of ≈20% can be reached.^[1,15] Therefore, a thorough evaluation of the electronic properties and the factors controlling the low V_{OC} is highly essential to make progress with the conversion efficiency of FeS₂ solar cells.

The article is divided into two parts. In the first part, we concisely discuss fundamental electronic properties, surface state kinetics, and related surface conduction phenomena. This will build a necessary background to the second part where we discuss the provoking mechanisms for photovoltage loss. Finally, we conclude with some future research recommendations for key areas relevant for further understanding and to advance FeS₂ as a candidate thin-film PV material.

2. Fundamentals of Electronic Properties and Surface State Kinetics in FeS₂

Pyrite is a *d*-band semiconductor that belongs to the space group Pa-3. Its crystal structure comprises of two interpenetrating cation (Fe²⁺) and anion (S₂²⁻) in face-centered-cubic (fcc) sublattices. Each Fe²⁺ ion in the bulk is octahedrally coordinated (symmetry group O_h) by one of the sulfur atoms in a S₂²⁻ pair and positioned at the face of the cube. Because of a

strong ligand field, the metal *d* states split into nonbonding, triply degenerate Fe 3d t_{2g} states (d_{xy}, d_{yz}, and d_{zx}), and doubly degenerate Fe 3d e_g (d_{x²-y²} and d_{z²}) states. The valence band (VB) consists of Fe 3d t_{2g} states, and the conduction band (CB) minimum consists of Fe 3d e_g states hybridized with S *ppσ** orbitals (see Figure 1).^[12] FeS₂ has an indirect bandgap with a direct bandgap very close in energy. In the literature, the reported bandgap of bulk FeS₂ vary between 0.83 and 1.01 eV,^[16] while the mostly cited bandgap is ≈0.95 eV.^[17]

On a fractured FeS₂, neutral sulfur vacancies (S-vacancies) contribute dominantly in formation of the surface states. Significant concentrations of S-vacancies have been measured in pyrite faces by X-ray diffraction, photoelectron spectroscopy, and thermogravimetric data.^[1,3] Therefore, the degree of off-stoichiometry of FeS₂ may be predicted by the equilibrium concentration of its native defects due to S-vacancies. According to density functional theory (DFT) calculations, the magnitude of the S-vacancies decays almost entirely to zero beyond approximately three atomic layers into the bulk.^[11]

Due to S-deficiencies, FeS₂ undergoes a reduction in symmetry from octahedral (O_h) toward square pyramidal (C_{4v}). This symmetry reduction leads to a loss of degeneracy among the Fe 3d t_{2g} and bandgap states.^[18] Therefore, a reduction in the bandgap was anticipated in the presence of these surface states.^[17] Zhang et al. theoretically predicted a maximum bandgap of 0.56–0.71 eV for S-deficient, and 0–0.3 eV for S-rich surfaces.^[19] Other authors have theoretically calculated that S-vacancies may turn the bandgap to zero by making the surface metallic.^[11] The small V_{OC} in single crystals FeS₂ solar cell has therefore been associated with S-vacancies.^[20]

The kinetics of the formation of S-vacancies was studied by many groups using DFT.^[11,19,21] DFT results predicted high formation energies for defects due to S-vacancies. It means that a high concentration of defects formation within the FeS₂ crystal is not probable. This clearly contradicts the experimental finding of considerable amounts of defects and in consequence, the ability for facile S-vacancy formation in FeS₂ needs to be revisited. It is to be noted that synthesis techniques, however, have progressed in a level to synthesize phase pure pyrites.^[22] Birkholz et al. reported that pyrite samples are S-deficient up to 13 at%.^[20] Contrarily, Ellmer and Höpfner have argued that reports of Birkholz et al. are likely to be a measurement error as they believe the S-deficiency of pyrite should be within 1 at%.^[23]

Because of this and aforementioned contradictory data, the amount and nature of S-deficiencies in FeS₂ remain uncertain.

The presence of S-vacancies in FeS₂ is undeniable, regardless of the debate whether it appears in high or low concentration. Research has therefore invested in understanding FeS₂ surfaces related electronic behavior, notably, the surface conduction in FeS₂. The surface conductive layer is commonly assigned with a p-type behavior, while bulk is n-type.^[7,13] This surface inversion suggests pinning of the surface Fermi level near the valence band edge.^[7] Bronold et al. reported that the fivefold surface coordination of Fe causes the Fe 3d_{z²} (e_g) orbital to fall into the bandgap, and thus creating an intrinsic surface state,^[24] which was shown as a likely cause of the origin of the p-type surface and associated Fermi level pinning near the valence band.^[24,25]

3. Current Trends in Understanding of the Origin of Low Photovoltage in FeS₂ Solar Cells

Extensive research efforts of last 35 years made a significant progress in synthesis and understanding of surface-related electronic and optical properties of FeS₂. Nevertheless, solar energy conversion efficiency for FeS₂ solar cell has remained below 2.8%. A low V_{OC} in this case is the ultimate reason for this poor the efficiency. Therefore, a mechanistic understanding of the photovoltage loss mechanisms is highly essential.

In early nineties of last century, a hypothesis was made that this low V_{OC} could be due to an electronic defect coupled to the material.^[20] The intrinsic surface states were postulated to cause Fermi level pinning at the space charge region (SCR) and limit the barrier height in the SCR. Therefore, although not fully understood, surface Fermi level pinning was hypothesized as the major reasons for photovoltage loss in FeS₂.^[26] This hypothesis gained importance when an investigation revealed that both natural and synthetic crystals were found to be exclusively sulphur deficient.^[27]

Later on, it was contested that pinning of surface Fermi level at an energy level to limit the barrier height significantly is unlikely to happen. Instead, it was reported that the Fermi level is intrinsically pinned near the valence band maximum of FeS₂ single crystals, due to charge neutrality condition caused by the equilibration of the bulk Fermi level with a high density of surface acceptor states.^[32] As a result, band bending (and therefore, the barrier height) should be large. It implies that Fermi level pinning instead should work toward an increase in measured V_{OC}. It was further argued that when the Fermi level is pinned, negatively charged surface states should be spatially separated from the positive space charge region—resulting in charge accumulation to form a Schottky buried junction. It consequently would mediate and facilitate the extraction of photogenerated minority carriers across the interface.^[10] It means that Fermi level pinning due to surface states only cannot satisfactorily explain the low V_{OC} and limited performance of FeS₂ solar cells.

To advance the understanding of photovoltage loss, recently, formation of a hole-rich inversion layer at the surface has been accounted for as a source of photovoltage loss in pyrite photocells (see **Figure 2**).^[28] The low voltage was believed to be caused by thermionic field emission through a thin triangular potential

barrier at the surface of the crystal (**Figure 2b**).^[25] The symmetry reduction (distorted octahedral to square pyramidal coordination) due to change in iron coordination number (from six to five) at the surface was shown to be the likely origin of this thermionic emission. The symmetry reduction leads to creation of surface states at energies close to the valence band edge. When the Fermi level of the n-type bulk tends to equilibrate with surface states, it creates a strong upward band bending and an inversion layer. As a result, donors near the surface rise above the Fermi level and are ionized. This consequently enhances the surface field to create a thin triangular potential barrier for direct tunneling of majority carriers (**Figure 2d**). This leaky potential barrier can be a possible origin for the large dark current, and therefore loss of charges and subsequently limiting the V_{OC}.^[7,9]

Bronold et al. predicted the likely existence of an inversion layer at the surface of pyrite.^[24,25] Later on, Law et al. made the intensive studies on emergence of surface states induced hole-rich surface inversion/accumulation layer,^[7,28,29] which is subsequently expounded by Aydil and Leighton et al.^[3,13] Surface conduction in pyrite single crystals dominates at temperatures low enough to freeze out a sufficient fraction of the bulk electrons, while in pyrite thin films, it could happen at all temperatures because of a large surface to volume fraction.^[7,9]

The inversion layer is caused by large upward band bending at the surface due to the ionization of holes from a shallow surface acceptor to the valence band. Existence of a hole-rich inversion layer at the surface of the n-type crystals was demonstrated with Hall measurements.^[7] Unusual sign changes have also been noticed for the Hall coefficient (R_H), see **Figure 2c**. It was shown that while electrons in the bulk of the crystal are frozen out at low temperatures, the holes in the inversion layer become dominating for the conduction.^[33] It indicates that a parallel conduction would be possible with a p-type surface and an n-type bulk, at least at low temperatures. When the temperatures reach close to the |R_H| maximum, a regime of mixed transport between bulk electrons and surface holes appears. In this case, the spatial separation of these charge carriers is maintained by the surface electric field.^[32] The inversion layer is therefore electrically isolated from the n-type bulk by a depletion region.

In addition to the concept of surface inversion, an alternative hypothesis based on the ionization of deep donor states at bulk has been proposed for photovoltage loss in FeS₂.^[10] The origin of these donor states in the bulk is related to the intrinsic sulfur vacancies and reduction of the Fe–S coordination in FeS₂. Ionized deep donor states would contribute in recombination of conduction band electrons with photogenerated holes in valence band by direct band–band relaxation or by tunneling toward the interface. Therefore, ionized donor states have shown to affect the homogeneity of charge density distribution in the SCR and the barrier height at the intrinsic surface Fermi level (see **Figure 3a,b**).^[10]

Inhomogeneous charge distribution due to deep ionized donor states resulted in SCR with two distinct regimes, namely, nonconstant regime and abrupt regime (see **Figure 3b**). A nonconstant regime was defined for the potentials within bulk Fermi level and half occupancy (F1/2) of the deep donor band based on the Fermi–Dirac distribution, while an abrupt regime was defined beyond half occupancy (F1/2). Therefore, singly

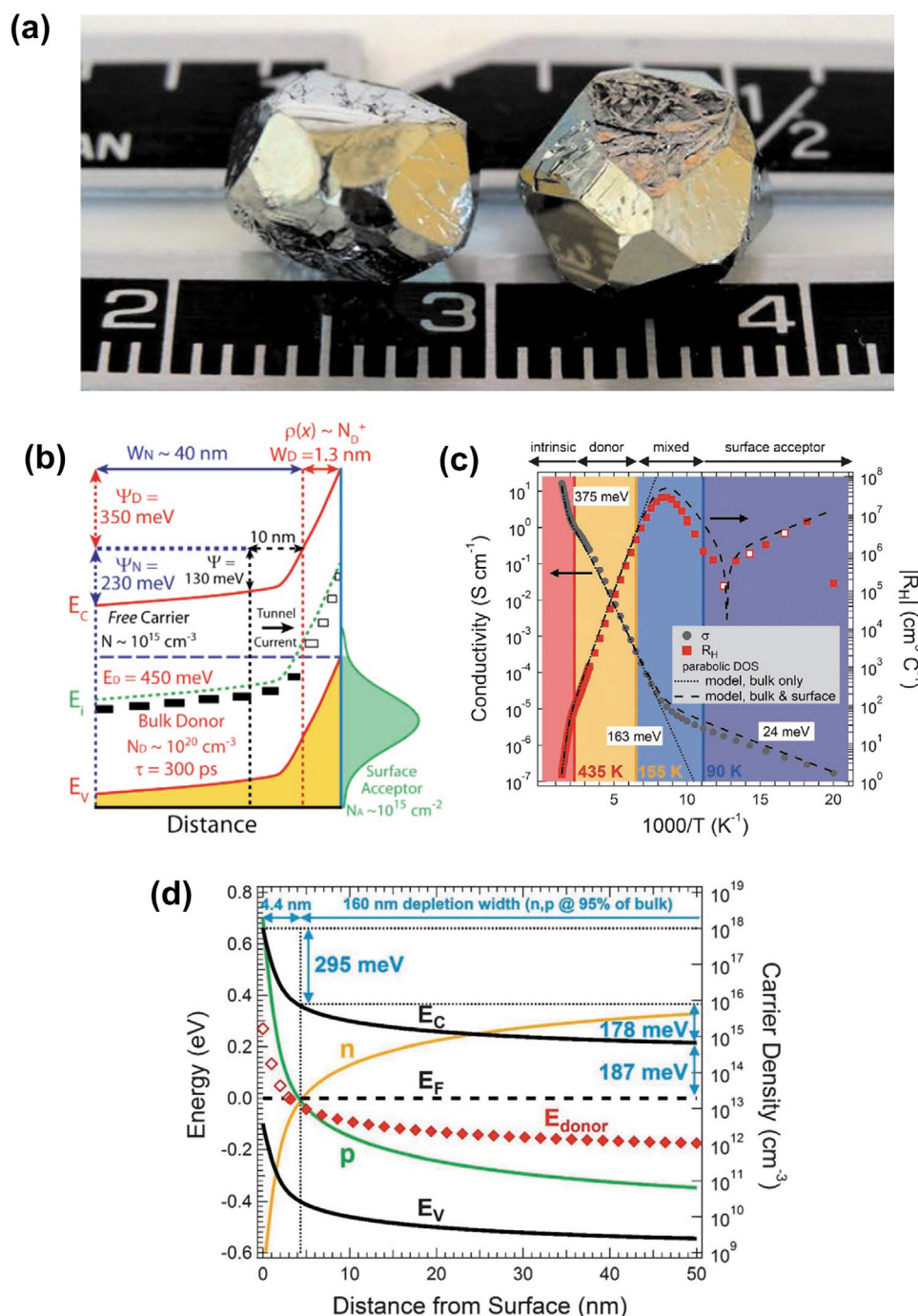


Figure 2. a) Photograph of as-grown FeS₂ crystals. Scale is in centimeters. b) Space charge region properties of the iron pyrite single crystals. Occupancy of the deep donor (N_D) density of states (DOS) relative to the bulk and surface Fermi level and energy band scheme for (100)-faceted iron pyrite single crystal. c) Hall measurements (σ and $|R_H|$) for a pyrite. Three linear regions with activation energies are shown. The Hall coefficient exhibits unusual behavior, including a minimum at ≈ 120 K and a sign change from negative (electron dominant) to positive (hole dominant) at ≈ 80 K. The red squares indicate negative values of R_H , while the red and white squares are positive values. The sign of R_H varies at low temperature because the Hall voltage V_H is very small in this regime. The dotted traces show data fitted with numerical modelling. d) Calculated equilibrium band diagram of the pyrite surface at 300 K. a,c,d) Adapted with permission.^[7] Copyright 2014, Royal Society of Chemistry. b) Adapted with permission.^[10] Copyright 2014, American Chemical Society.

occupied deep donor states form the nonconstant charge distribution in the SCR, and fully ionized donor states form the abrupt region. Understandably, in the nonconstant regime,

charge density follows the ionization of deep donor states, while it equals the concentration of deep donor states in the abrupt regime. The experimental profile of abrupt SCR (1.3 nm)

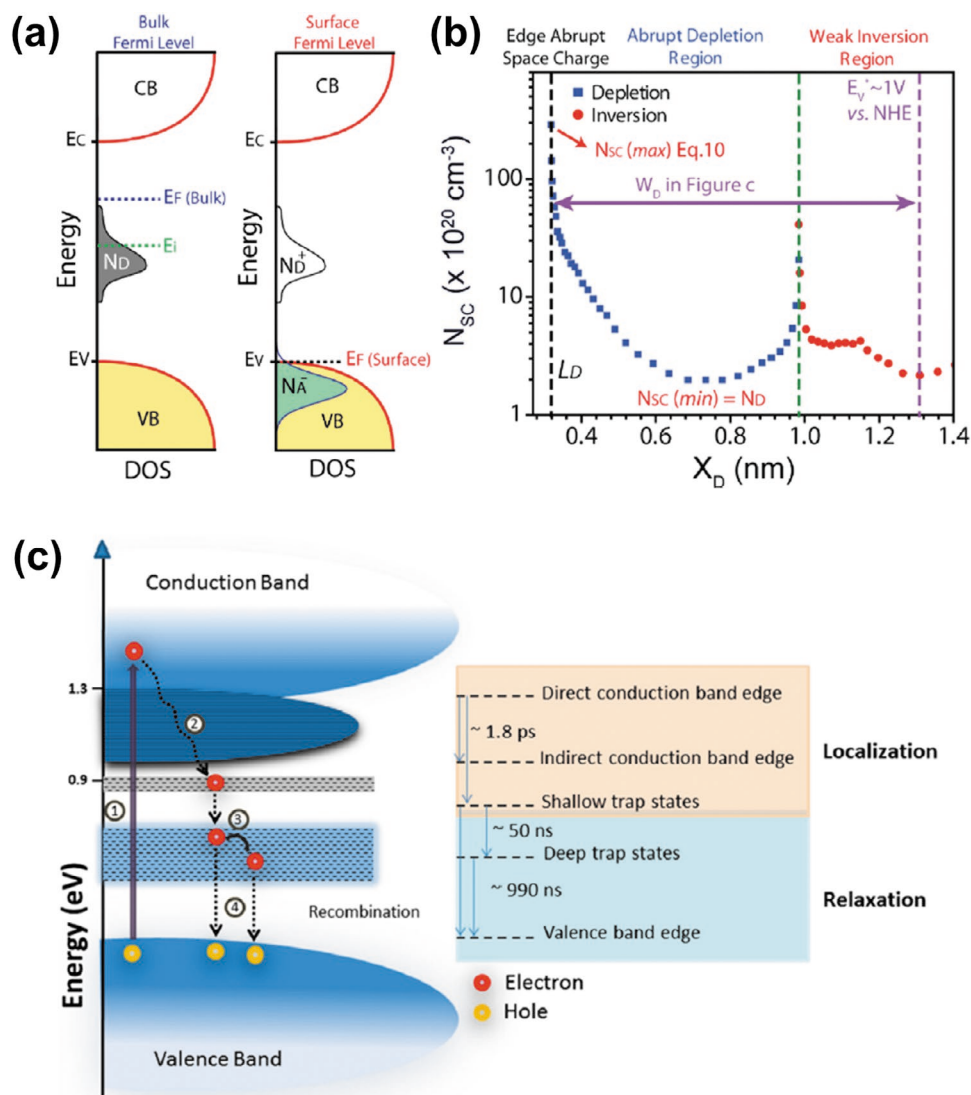


Figure 3. Space charge region properties of the iron pyrite single crystals. a) Occupancy of surface acceptor states (N_A) and deep donor (N_D) density of states (DOS) relative to the bulk and surface Fermi level. b) Experimental profile for the apparent charge density in the abrupt space charge region (N_{SC}) as a function of the variable abrupt space charge depth (X_D) which is shown using a purple double-sided arrow. c) Schematic of the photophysical processes involved in iron pyrite based on optical pump probe spectroscopy. Here, 1: optical excitation of electron from valence to conduction band, 2: rapid carrier localization of the excited carrier to indirect band edge and low lying shallow defect states, 3: slower electron relaxation to midgap deep defect states/band (long lived trap states), and 4: electron recombination process with the valence band holes. a,b) Adapted with permission.^[10] Copyright 2014, American Chemical Society. c) Adapted with permission.^[14] Copyright 2016, American Chemical Society

is accompanied with depletion region (1 nm) and weak inversion region (0.3 nm).^[10] These regions govern the charge distribution and width of SCR with the change of the Fermi level position respective to valence band edge. This very narrow abrupt surface charge region has shown to introduce surface tunneling and impose a limitation to barrier height of ≈ 230 mV, and consequently resulted in a limited V_{OC} .

Recently, research efforts have been made to understand the fundamental limitation of V_{OC} by quantifying the photocarrier loss in high quality and phase pure iron pyrite cubes.^[14] Photocarriers are shown to be lost due to fast carrier localization of photoexcited carriers to indirect band edge and shallow trap states. Ligand field theory and molecular orbital theory predict

the formation of midgap defect states/band due to S-vacancies. Defect states within the bandgap therefore can influence the carrier dynamics and the optoelectronic performance.^[30]

Transient absorption spectroscopy of iron pyrite nanocubes revealed a band edge photo-bleaching and below bandgap photoinduced absorption as representing cases of disorder and defect-assisted charge carrier trapping and recombination (see Figure 3c).^[14] The photo-bleaching signal originates from near bandgap stimulated emission of the photogenerated carriers and state-filling of the band edge states, while the below bandgap photoinduced absorption band originates from the localized charge carrier absorption. The observed fast decay of photo-bleaching was interpreted as the localization of

photogenerated charge carrier at the band edge and midgap trap states. The resulted photocarrier losses therefore have been postulated as a dominant reason for the photovoltage loss in iron pyrite.^[14]

4. Conclusions and Future Perspective

We are in a dire need of having earth abundant, nontoxic and low-cost materials made into thin-film technologies beyond widely used Si for next generation solar cells to meet a more sustainable and low energy production approach for residential, commercial, and industrial uses. Regardless of the conversion efficiency, the most important parameter is the cost per Watt of electricity production. To this context, FeS₂ has the true potential to be the deal breaker, but still faces several challenges. The grand challenge is to significantly increase the solar energy conversion efficiency for FeS₂ solar cells to more than 3%. Despite significant progress in synthesis and characterization, the V_{OC} for a cell with appreciable amount of photocurrent is still limited to <0.2 V. Therefore, a clear understanding of the origin of low V_{OC} in FeS₂ is highly important to overcome the limitation in the efficiency of next generation pyrite based solar cells.

We have discussed the past debates and current progress in understanding the mechanisms of photovoltage loss in FeS₂, which we believe is essential to unlock the full PV potential of this material. By synthesizing the literature, it might be concluded that available mechanisms to understand photovoltage loss have their own limitations, and eventually cannot stand out solid to definitively explain the origin of low V_{OC} . It is also to be noted at the same time that in the midst of a great volume of fundamental research reports available on FeS₂ (>thousands), there are only few reports (<15) that have demonstrated a photovoltage in a device.^[6,7,10,14,31] This article may therefore provide the impetus for more advanced and customized studies to unveil the origin of the commonly low V_{OC} in FeS₂. We here below discuss some challenges remained and new research directions that may be pursued for improved understanding and performance of FeS₂.

Surface and bulk states play significant roles in the photovoltage. Surface inversion, leaky potential barrier, tunneling majority carrier, photocarrier loss, nonconstant charge distribution, very narrow space charge region, and so on, all are related to the surface and bulk states. It is estimated that if donor states could reduce below $\approx 10^{17}$ cm⁻³, thermionic emission would become insignificant and enhance the maximum V_{OC} above 450 mV.^[7] Despite a noticeable progress in synthesis of phase pure pyrite crystals/films,^[7-9,14,28,29,32] challenges remain in reducing the concentration of surface states and bulk donor states below 10¹⁹ cm⁻³. Passivation of surface states and near surface states may be one possible way to overcome this.^[33]

Depending on the synthesis conditions, pyrite phase of FeS₂ often incorporates one or more of the secondary phases. Sulfur-deficient metallic iron sulfides (e.g., troilite FeS, pyrrhotite Fe_{1-x}S, smythite Fe₉S₁₁, greigite Fe₃S₄, etc.) and orthorhombic marcasite (FeS₂) are the most notable secondary phases. However, considering the comparable free energy of formation and small difference in relative stability, coexistence of marcasite with either natural or synthetic pyrite is highly

probabilistic.^[12,34] These secondary phases when present in conjugation with the pyrite structures are supposedly considered detrimental for pyrite-based solar cell performance, while marcasite phase has been reported to be the most deleterious.^[35]

Traditionally, the smaller bandgap (0.34 eV) of marcasite was believed to impede the development of photovoltage.^[1] However, there is an inconsistency in the reported values for the bandgap of marcasite which varies between 0.3 and 1.6 eV.^[1,36,37] Therefore, the low bandgap cannot be faithfully ascribed to be the reason for lower photovoltage developed in pyrite solar cells. In contrast, recently, the coexistence of marcasite with pyrite phase has been reported beneficial for improved photoresponse and photocurrent.^[36] Because of the band alignment, it was reported that a mixed phase of marcasite/pyrite established a junction that facilitated efficient charge separation.

On the other hand, synthesis of pyrite can be fine-tuned to avoid metallic phases completely,^[38] and therefore, they are apparently not a matter of high concern.^[35] The reality is that research has been directed to speculate the impact of the secondary phases. However, these speculations have not yet been supported by real data while measuring the cell efficiency.

Several DFT and experimental studies speculated that the narrowing of the bandgap of the pyrite surface might cause the photovoltage loss in pyrite devices.^[7,11,17,19,1,39] However, there is the uncertainty in the calculated/measured values of bandgap. More sophisticated experiment needs to be designed (e.g., combining ultraviolet photoemission, inverse photoemission, scanning tunnelling spectroscopy, etc.) to definitively establish the bandgap of pyrite surfaces.

The orientation/reorientations of anions in FeS₂ around their average lattice position or ion exchange may result in dynamic disorder in crystal structure. The cooling and transport of photoexcited charge carriers depend on this lattice dynamics. As a result, the coupling between electronic excitations and lattice vibrations (i.e., electron-phonon interactions) is influenced by lattice dynamics.^[40] Solar cell is an optoelectronic device that interfaces with both optical and electrical properties.^[41] In nanoscale electronic devices, the dominating source of energy loss comes from impurity scattering associated with extrinsic doping, while electron-phonon coupling is the second largest source of loss in optoelectronic devices and can significantly affect the electronic conductivity and energy efficiency.^[42] Different from the Coulombic or charge interactions involved with ionized impurity scattering, phonon scattering couples exciton energy into a phonon wave. Therefore, electron-phonon coupling is important for electronic transport properties of optoelectronic devices at the nanoscale and is also connected to the subsequent thermalization process of charge carriers. Nanostructures, because of their confined nature, are more susceptible to electron-phonon coupling down to a size where there are suppression of phonons, where instead undercoordinated surface groups and dangling bonds can give rise to soft-modes and molecular vibrations and other pathways to energy loss. Evidently, bulk phonons and surface vibrations are the most likely sources reducing carrier mobilities, and are unavoidable.^[42]

Particularly, phonon lifetimes are critically important as they provide insight into both electron-phonon and

phonon–phonon scattering. For example, if phonons are slow to dissipate heat, it will create nonequilibrium phonon populations that will consequently affect carrier relaxation and scattering processes.^[40,43] Therefore, interaction of phonons with charge carriers has substantial effects on the operation of solar cells. Phonons are quantized vibrational mechanical energy, and result in inelastic Raman interactions between photons and the lattice. Raman spectroscopy under near resonant excitation (where the incident photon energy is near the material's bandgap) should therefore be useful technique to extract electron–phonon coupling strengths.^[42] Additionally, neutron scattering measurements may be exploited to deduce the phonon lifetimes in bulk to scale the contribution of specific phonon modes to the thermal conductivity.^[40]

We also envisage that efficiency of FeS₂ solar cells might be increased by photon recycling, or by controlling the spectral or angular emission from the cell. These techniques were proven effective for other kinds of solar cells.^[44,45] These can be realized by integrating external component in solar cell architecture. For example, adding a selective reflector to a cell, conceptually, can surpass bandgap limitation.^[44] The idea is to feed back the band edge emitted photons into the device by the reflectors to build up the effective quasi Fermi level of the electrons that would allow emission above the threshold of bandgap.

However, electron–phonon coupling and photon recycling are recommended here for more advanced research, given that respectable efficiencies are routinely obtained. With critical analysis of previous findings and more detailed investigations and suppression of the energy loss mechanisms, we believe that it would not be impossible to obtain a high photovoltage with FeS₂ solar cells one day.

Acknowledgements

The authors acknowledge the generous support from Swedish Energy Agency (Grant No. 44648-1).

Conflict of Interest

The authors declare no conflict of interest.

Keywords

defects, electronic structure, iron pyrite, open-circuit voltage, solar cells

Received: August 30, 2019
Revised: November 28, 2019
Published online: May 19, 2020

- [1] A. Ennaoui, S. Fiechter, C. Pettenkofer, N. Alonso-Vante, K. B ker, M. Bronold, C. H pfner, H. Tributsch, *Sol. Energy Mater. Sol. Cells* **1993**, *29*, 289.
[2] R. Schieck, A. Hartmann, S. Fiechter, R. K nenkamp, H. Wetzlar, *J. Mater. Res.* **1990**, *5*, 1567.
[3] B. Voigt, W. Moore, M. Manno, J. Walter, J. D. Jeremiason, E. S. Aydil, C. Leighton, *ACS Appl. Mater. Interfaces* **2019**, *11*, 15552.

- [4] C. Wadia, A. P. Alivisatos, D. M. Kammen, *Environ. Sci. Technol.* **2009**, *43*, 2072.
[5] a) P. P. Altermatt, T. Kiesewetter, K. Ellmer, H. Tributsch, *Sol. Energy Mater. Sol. Cells* **2002**, *71*, 181; b) K. Morita, T. Miki, *Intermetallics* **2003**, *11*, 1111.
[6] A. Ennaoui, H. Tributsch, *Sol. Cells* **1984**, *13*, 197.
[7] M. Limpinsel, N. Farhi, N. Berry, J. Lindemuth, C. L. Perkins, Q. Lin, M. Law, *Energy Environ. Sci.* **2014**, *7*, 1974.
[8] M. Cab n-Acevedo, D. Liang, K. S. Chew, J. P. DeGrave, N. S. Kaiser, S. Jin, *ACS Nano* **2013**, *7*, 1731.
[9] D. Liang, M. Caban-Acevedo, N. S. Kaiser, S. Jin, *Nano Lett.* **2014**, *14*, 6754.
[10] M. Caban-Acevedo, N. S. Kaiser, C. R. English, D. Liang, B. J. Thompson, H. E. Chen, K. J. Czech, J. C. Wright, R. J. Hamers, S. Jin, *J. Am. Chem. Soc.* **2014**, *136*, 17163.
[11] L. Yu, S. Lany, R. Kykyneshi, V. Jieratum, R. Ravichandran, B. Pelatt, E. Altschul, H. A. S. Platt, J. F. Wager, D. A. Keszler, A. Zunger, *Adv. Energy Mater.* **2011**, *1*, 748.
[12] R. Sun, M. K. Y. Chan, G. Ceder, *Phys. Rev. B* **2011**, *83*, 235311.
[13] a) J. Walter, X. Zhang, B. Voigt, R. Hool, M. Manno, F. Mork, E. S. Aydil, C. Leighton, *Phys. Rev. Mater.* **2017**, *1*, 065403; b) X. Zhang, M. Li, J. Walter, L. O'Brien, M. A. Manno, B. Voigt, F. Mork, S. V. Baryshev, J. Kakalios, E. S. Aydil, C. Leighton, *Phys. Rev. Mater.* **2017**, *1*, 015402.
[14] S. Shukla, G. Xing, H. Ge, R. R. Prabhakar, S. Mathew, Z. Su, V. Nalla, T. Venkatesan, N. Mathews, T. Sritharan, T. C. Sum, Q. Xiong, *ACS Nano* **2016**, *10*, 4431.
[15] W. Shockley, H. J. Queisser, *J. Appl. Phys.* **1961**, *32*, 510.
[16] D. Banjara, Y. Malozovsky, L. Franklin, D. Bagayoko, *AIP Adv.* **2018**, *8*, 025212.
[17] F. W. Herbert, A. Krishnamoorthy, K. J. Van Vliet, B. Yildiz, *Surf. Sci.* **2013**, *618*, 53.
[18] R. Sun, M. K. Y. Chan, S. Kang, G. Ceder, *Phys. Rev. B* **2011**, *84*, 035212.
[19] Y. N. Zhang, J. Hu, M. Law, R. Q. Wu, *Phys. Rev. B* **2012**, *85*, 085314.
[20] M. Birkholz, S. Fiechter, A. Hartmann, H. Tributsch, *Phys. Rev. B* **1991**, *43*, 11926.
[21] a) A. Krishnamoorthy, F. W. Herbert, S. Yip, K. J. Van Vliet, B. Yildiz, *J. Phys. Condens. Matter.* **2013**, *25*, 045004; b) F. W. Herbert, A. Krishnamoorthy, W. Ma, K. J. Van Vliet, B. Yildiz, *Electrochim. Acta* **2014**, *127*, 416.
[22] a) D. R. Cummins, H. B. Russell, J. B. Jasinski, M. Menon, M. K. Sunkara, *Nano Lett.* **2013**, *13*, 2423; b) H. A. Macpherson, C. R. Stoldt, *ACS Nano* **2012**, *6*, 8940; c) X. Mao, J. G. Kim, J. Han, H. S. Jung, S. G. Lee, N. A. Kotov, J. Lee, *J. Am. Chem. Soc.* **2014**, *136*, 7189.
[23] K. Ellmer, C. H pfner, *Philos. Mag. A* **1997**, *75*, 1129.
[24] M. Bronold, Y. Tomm, W. Jaegermann, *Surf. Sci.* **1994**, *314*, L931.
[25] M. Bronold, C. Pettenkofer, W. Jaegermann, *J. Appl. Phys.* **1994**, *76*, 5800.
[26] S. F. A. Ennaoui, W. Jaegermann, H. Tributsch, *J. Electrochem. Soc.* **1986**, *133*, 97.
[27] J. Luck, A. Hartmann, S. Fiechter, *Fresenius' Z. Anal. Chem.* **1989**, *334*, 441.
[28] N. Berry, M. Cheng, C. L. Perkins, M. Limpinsel, J. C. Hemminger, M. Law, *Adv. Energy Mater.* **2012**, *2*, 1124.
[29] S. Seefeld, M. Limpinsel, Y. Liu, N. Farhi, A. Weber, Y. Zhang, N. Berry, Y. J. Kwon, C. L. Perkins, J. C. Hemminger, R. Wu, M. Law, *J. Am. Chem. Soc.* **2013**, *135*, 4412.
[30] a) B.-w. Park, X. Zhang, E. M. J. Johansson, A. Hagfeldt, G. Boschloo, S. I. Seok, T. Edvinsson, *Nano Energy* **2017**, *40*, 596; b) M. Pazoki, T. J. Jacobsson, J. Kullgren, E. M. Johansson, A. Hagfeldt, G. Boschloo, T. Edvinsson, *ACS Nano* **2017**, *11*, 2823.
[31] a) A. Ennaoui, S. Fiechter, H. Tributsch, M. Giersig, R. Vogel, H. Weller, *J. Electrochem. Soc.* **1992**, *139*, 2514; b) A. Kirkeminde, R. Scott, S. Ren, *Nanoscale* **2012**, *4*, 7649; c) Y. C. Wang, D. Y. Wang, Y. T. Jiang, H. A. Chen, C. C. Chen, K. C. Ho, H. L. Chou,

- C. W. Chen, *Angew. Chem., Int. Ed.* **2013**, *52*, 6694; d) C. Steinhagen, T. B. Harvey, C. J. Stolle, J. Harris, B. A. Korgel, *J. Phys. Chem. Lett.* **2012**, *3*, 2352; e) Y. Bi, Y. Yuan, C. L. Exstrom, S. A. Darveau, J. Huang, *Nano Lett.* **2011**, *11*, 4953; f) S. Shukla, N. H. Loc, P. P. Boix, T. M. Koh, R. R. Prabhakar, H. K. Mulmudi, J. Zhang, S. Chen, C. F. Ng, C. H. Huan, N. Mathews, T. Sriharan, Q. Xiong, *ACS Nano* **2014**, *8*, 10597.
- [32] a) J. M. Lucas, C.-C. Tuan, S. D. Lounis, D. K. Britt, R. Qiao, W. Yang, A. Lanzara, A. P. Alivisatos, *Chem. Mater.* **2013**, *25*, 1615; b) M. Cabán-Acevedo, M. S. Faber, Y. Tan, R. J. Hamers, S. Jin, *Nano Lett.* **2012**, *12*, 1977; c) L. Samad, M. Cabán-Acevedo, M. J. Shearer, K. Park, R. J. Hamers, S. Jin, *Chem. Mater.* **2015**, *27*, 3108; d) B. B. Yu, X. Zhang, Y. Jiang, J. Liu, L. Gu, J. S. Hu, L. J. Wan, *J. Am. Chem. Soc.* **2015**, *137*, 2211; e) F. Jiang, L. T. Peckler, A. J. Muscat, *Cryst. Growth Des.* **2015**, *15*, 3565; f) J. Puthusseray, S. Seefeld, N. Berry, M. Gibbs, M. Law, *J. Am. Chem. Soc.* **2011**, *133*, 716.
- [33] a) M. Z. Rahman, S. I. Khan, *Mater. Renewable Sustainable Energy* **2012**, *1*, 1; b) M. Z. Rahman, *Renewable Sustainable Energy Rev.* **2014**, *30*, 734.
- [34] V. K. Gudelli, V. Kanchana, S. Appalakondaiah, G. Vaitheeswaran, M. C. Valsakumar, *J. Phys. Chem. C* **2013**, *117*, 21120.
- [35] M. Z. Rahman, T. Edvinsson, *Joule* **2019**, *3*, 2290.
- [36] a) L. Wu, N. Y. Dzade, L. Gao, D. O. Scanlon, Z. Ozturk, N. Hollingsworth, B. M. Weckhuysen, E. J. Hensen, N. H. de Leeuw, J. P. Hofmann, *Adv. Mater.* **2016**, *28*, 9602; b) D. G. Moon, S. Rehan, S. Y. Lim, D. Nam, I. Seo, J. Gwak, H. Cheong, Y. S. Cho, Y. Lee, S. Ahn, *Sol. Energy* **2018**, *159*, 930.
- [37] D. G. Moon, A. Cho, J. H. Park, S. Ahn, H. Kwon, Y. S. Cho, S. Ahn, *J. Mater. Chem. A* **2014**, *2*, 17779.
- [38] S. Kment, H. Kmentova, A. Sarkar, R. J. Soukup, N. J. Ianno, D. Sekora, J. Olejnicek, P. Ksirova, J. Krysa, Z. Remes, Z. Hubicka, *J. Alloys Compd.* **2014**, *607*, 169.
- [39] P. Lazic, R. Armiento, F. W. Herbert, R. Chakraborty, R. Sun, M. K. Chan, K. Hartman, T. Buonassisi, B. Yildiz, G. Ceder, *J. Phys.: Condens. Matter* **2013**, *25*, 465801.
- [40] A. Gold-Parker, P. M. Gehring, J. M. Skelton, I. C. Smith, D. Parshall, J. M. Frost, H. I. Karunadasa, A. Walsh, M. F. Toney, *Proc. Natl. Acad. Sci. USA* **2018**, *115*, 11905.
- [41] M. Z. Rahman, T. Edvinsson, *Matter* **2019**, *3*, 556.
- [42] J. K. Marmon, *Ph.D. Thesis*, The University of North Carolina at Charlotte, Charlotte, NC, USA **2016**.
- [43] M. B. Price, J. Butkus, T. C. Jellicoe, A. Sadhanala, A. Briane, J. E. Halpert, K. Broch, J. M. Hodgkiss, R. H. Friend, F. Deschler, *Nat. Commun.* **2015**, *6*, 8420.
- [44] A. Niv, Z. R. Abrams, M. Gharghi, C. Gladden, X. Zhang, *Appl. Phys. Lett.* **2012**, *100*, 083901.
- [45] O. D. Miller, E. Yablonovitch, S. R. Kurtz, *IEEE J. Photovoltaics* **2012**, *2*, 303.